RSC Advances

Journal Name

ARTICLE

Shape Controlled Synthesis of Multi-Branched Gold Nanocrystals Through a Facile One-Pot Bifunctional Biomolecular Approach

M. Sajitha,[a,b] A. Vindhyasarumi,[a] A. Gopi[a,b] and K. Yoosaf [*a,b]

Anisotropic nanocrsytals of gold and silver are promising candidates for sensing and therapeutic applications because of their high extinction coefficient, increased NIR response and localization of hot spots at their tips. Herein, we report a viable room temperature synthetic strategy to prepare multi-branched gold nanocrystals of varying morphologies without the aid of additional nanoseeds or shape directing agents. By systematically modulating the bifunctional ligand to Au^{3+} ion molar ratio ([L-DOPA]/[HAuCl$_4$] = 0.15 - 1), the plasmon absorption was tuned from visible (530 nm) to NIR (930 nm). The corresponding microscopic studies showed a gradual transformation of the nanomaterial's morphology from multiply twinned spheres to branched stars and flowers. The detailed spectroscopic and microscopic studies have revealed that evolution of these branched nanocrystals proceeds through aggregation and subsequent overgrowth of initially produced spherical particles.

Introduction

Metal nanoparticles with multiple branches such as nanostars are gaining recent attention mainly because of their potential use in plasmonics and sensing platforms.[1-3] Surface plasmons and hence enhanced electric fields are localized at the tips of such nanostructures.[4-9] This results in more number of hot spots per nanoparticle and they exhibit very high extinction coefficients of the order of 10^8-10^9 M^{-1} cm^{-1}.[10] Due to these, single molecular sensitivity has been easily achieved with such materials.[11-13] Furthermore, increased NIR response makes them highly suitable for biomedical therapeutics such as photothermal therapy and bioimaging.[3,14] However, at present, only a few synthetic routes are available to prepare these promising classes of materials. The most common and well exploited methodologies include reduction of Au^{3+} ions in presence of nanoseeds, that are either citrate or NaBH$_4$ reduced, and shape directing agents like cetyltrimethylammonium bromide (CTAB),[15,16] polyvinylpyrrolidone (PVP)[17-19] and others.[20-22] Usually these surfactants form a capping layer around the nanoparticle surface and its toxicity limits their application in bio-medicinal

fields. Another efficient strategy is a seedless method, initially reported by J. Xie *et al.*, using Good's buffer in which 2-[4-(2-hydroxyethyl)-1-piperazinyl]ethanesulfonic acid (HEPES) acts both as reductant and shape directing agent.[23-25] There have been a few other literature reports on seedless approaches for nanostar synthesis. These include those prepared using stabilizers such as bis(p-sulfonatophenyl) phenylphosphine dihydrate dipotassium (BSPP),[26] polyethylene glycol (PEG),[27] polyvinylpyrrolidone (PVP),[17,28] lyotropic liquid crystal template,[22] hexadecylamine (HDA),[29] and a combination of AgNO$_3$ as shape directing agent and ascorbic acid as reducing agent.[30]

Phenolic compounds having multiple hydroxyl groups (e.g. hydroquinone, catechol etc.) are naturally occurring antioxidants. The redox potential of these classes of molecules usually appears below that of metal ions such as Au^{3+} and Ag^+ and hence could serve as good alternative and biocompatible reducing agents in the synthesis of metal nanoparticles. In one of the first examples, R. Baron *et al.* used neurotransmitters such as L-DOPA, dopamine etc. as the reductant, but in presence of CTAC capping ligand.[31] Later K. G. Thomas and coworkers demonstrated that another natural antioxidant, namely gallic acid, can function as a bifunctional ligand (reducing and stabilizing agent) in the synthesis of water soluble metal nanoparticles.[32] The Au and Ag nanoparticles thus produced were highly efficient in selective and naked eye detection of Pb^{2+} ions from aqueous media. Following this, several other groups investigated potentiality of many different natural phenolic antioxidants in the preparation of nanoparticles. The nanomaterials thus obtained are found to be highly biocompatible and suitable for sensing[33-35] and

[a.] Photosciences and Photonics Section, Chemical Sciences and Technology Division, CSIR-National Institute for Interdisciplinary Science and Technology, Thiruvananthapuram 695 019, Kerala, India.
[b.] Academy of Scientific and Innovative Research (AcSIR), New Delhi 110001, India.
† Footnotes relating to the title and/or authors should appear here.
Electronic Supplementary Information (ESI) available: [details of any supplementary information available should be included here]. See DOI: 10.1039/x0xx00000x

photothermal applications.[36,37] However, most of these efforts yielded spherical nanoparticles and preparation of more promising anisotropic nanostructures still remain a challenge. In a recent work, both the yield and tunability of Au nanorods in the seed mediated approach have shown to enhance when di/trihydroxybenzene or dopamine were employed as reductant and additive.[38,39] Similarly, there were also a few attempts to synthesize branched nanocrystals using these classes of molecules. Urchin like structures were obtained when hydroquinone was used as a secondary reducing agent along with citrate.[40] S. Yi *et al*. reported the formation of snowflake like Au nanoparticles[41] as a result of dopamine oxidative polymerization into highly branched polydopamine structures.[42] However, these reactions were carried out either in presence of nanoseeds or at boiling conditions. The resulting nanocrystals have the size of a few micrometers. Therefore, developing a simple room temperature synthetic methodology for multi-branched nanocrystals having size < 100 nm is highly desirable.

Herein, we illustrate, a simple one-pot procedure for the preparation of multi-branched gold nanocrystals using a bifunctional and bio-relevant molecule, namely L-3,4-dihydroxyphenylalanine (L-DOPA). The approach presented here is more environmentally benign as we are using one of the naturally occurring antioxidants which functions both as reducing and shape-directing agent. We also demonstrate tuning the size and morphology of the resulting nanocrystals from spherical to stars to flower by simple alteration of the reductant concentration.

Experimental

Materials and methods

Chemicals such as hydrogen tetrachloroaurate trihydrate (HAuCl$_4$.3H$_2$O) and L-3,4-dihydroxyphenylalanine (L-DOPA) were purchased from Ms. Sigma Aldrich. Sodium hydroxide was obtained from Ms. Sd fine Chem. Ltd. and were used as received without further purification. All glass wares were cleaned using aqua regia prior to use and the experiments were performed in Millipore water (18.2 MΩ).

UV-visible absorption spectra were obtained using a UV-3101PC UV-VIS-NIR (Ms. Shimadzu Corporation, JAPAN) and diode array UV-VIS 8453 (Ms. Agilent Technologies Inc. USA) spectrophotometers. All measurements were performed in quartz cuvette (1 cm).

For HRTEM studies, 10 μL of nanoparticle solution was drop casted onto a carbon coated Cu grid and imaged on a FEI's 300 kV high resolution (FEI-Tecnai G2-30 with EDAX) transmission electron microscope.

Dynamic light scattering (DLS) was carried out using Zetasizer nanoseries, (Zeta Nano–ZS, Ms. Malvern Instruments. UK). A minimum of six measurements were taken for each sample to ensure statistical significance. pH of the solution was monitored using Elico LI 612 pH analyser.

Samples for XRD were prepared by repeated drop casting of Au nanostar solutions onto a precleaned glass plate and data were acquired using a Panalytical PW 3040/60 X'Pert Pro powder diffractometer and Cu Kα1 radiation.

Results and discussion

The branched Au nanocrystals were synthesized by room temperature mixing of the bifunctional ligand L-DOPA with Au^{3+} ions in the presence of NaOH. Our control experiments revealed that the addition of NaOH is highly critical for the facile generation of nanoparticles (Fig. S1, ESI†). In a typical procedure, 0.13 mM L-DOPA and 0.1 mM NaOH were sequentially but quickly mixed with a 15 mL aqueous solution of HAuCl$_4$ (0.2 mM). The reaction mixture was shaken well and kept undisturbed. In about 20 minutes, solution developed wine red color indicating the formation of metal nanoparticles (inset of Fig. 1A). Interestingly, upon keeping the solution for further ~ 1 hour, its color gradually changed to purple. The corresponding optical measurements showed only a single absorption maximum centred around 530 nm in the initial stages. While two peaks (~530 nm and ~710 nm) were clearly evident after the colour change. In the case of the gold, isotropic spherical nanoparticles usually exhibit only one plasmon (centred around 520 nm) whereas anisotropic nanostructures such as nanorods, nanostars display multiple absorption maxima corresponding to different (transverse and longitudinal) modes of plasmon oscillation.[7-10,29,43-47] In order to understand the origin of these absorption spectral profiles and hence to characterize the produced nanoparticles, transmission electron microscopic (TEM) studies were performed. TEM images recorded from different areas of the sample confirmed the occurrence of more than 95 % multiply branched nanocrystals (Fig. 1B and Fig. S2, ESI†).

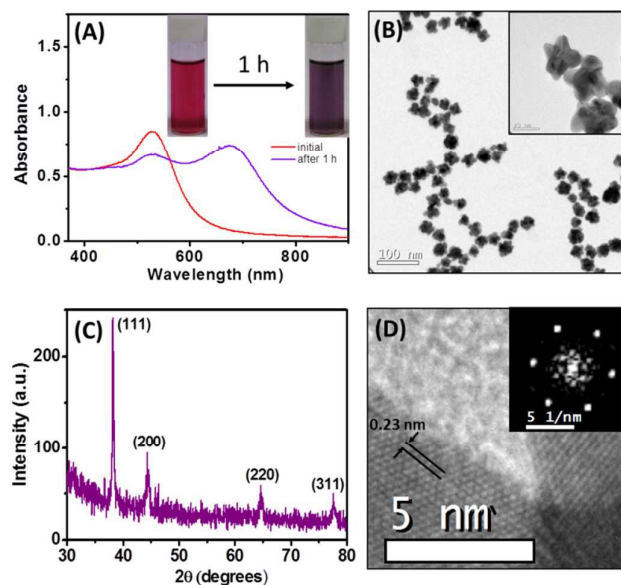Fig. 1 (A) Absorptionspectrum of Au nanoparticles in the initial stages (red) and after one hour (violet) prepared by adding 200 μM L-DOPA, Inset shows the colour photograph of the respective solutions (B) corresponding TEM images of the obtained nanostars (C) XRD data illustrating the crystal planes and (D) HRTEM images of the arms and inset shows the diffraction pattern obtained from one of the arms.
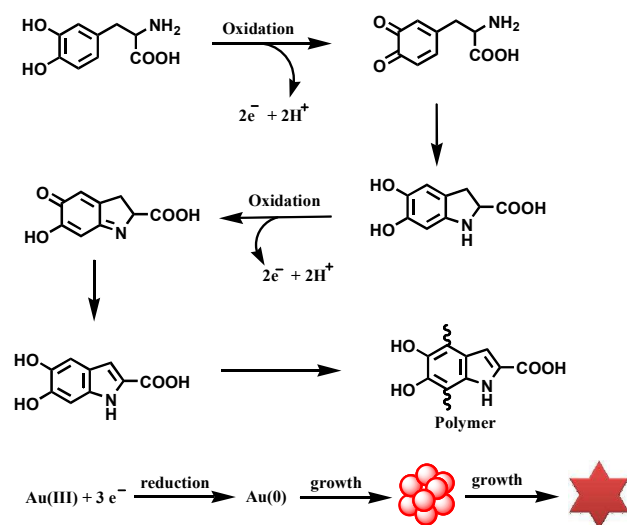
Scheme 1. Representation of L-DOPA oxidation and Au³⁺ reduction reactions resulting in the formation of polymer and branched Au nanocrystals.

The nanomaterials thus produced have size in the range 30-50 nm with majority having dimension ~35 nm (Fig. S3, ESI†). The no. of arms of the each nanocrystal varies from 3-7 and have a length of around 10 nm. The absorption properties of gold nanostars are known to arise from the combination plasmons localized at their core and tips.[48] In the present case, the absorption peak at ~ 530 nm (Fig. 1A) is mainly assigned to the transverse surface plasmon resonance (TSPR) of the core and tips. In addition this may also have contribution from any spherical particles present in the solution. While the lower energy band centred at ~710 nm arises from longitudinal surface plasmon resonance (LSPR) of the elongated branches.[8-10,29,43,45] From the HRTEM images the d spacing values were extracted as 0.235 nm and 0.201 nm (Fig. 1D). This corresponds to (111) and (200) planes of gold atoms in the fcc crystal lattice. Similar results were obtained from XRD measurements (Fig. 1C) which inferred the predominant (111) facets of nanocrystals.

Structurally, L-DOPA contains a catechol unit and zwitterionic amino acid part. Dihydroxy benzene unit of these types of biomolecules are known to undergo oxidation producing dopaquinone, dopachrome and other polymeric structures (Scheme 1).[42,49-51] The electrons released during this process can be involved in the reduction of metal cations. In the present case, the redox potential of L-DOPA is at least 0.3 V negative than Au(III)/Au(0) system and hence the reduction reaction is thermodynamically feasible.[52,53] It is reported that, the redox potentials of catechols shift to lower values with increase in pH.[53] Therefore, the rapid addition of NaOH raises the local pH, causing a faster reduction rate. The oxidized product thus produced may bind with nanoparticle surface and establish a capping layer. The IR spectrum of L-DOPA displayed numerous peaks corresponding to different modes of stretching and bending vibrations (Fig. S4, ESI†). Most of these peaks were absent in the IR spectrum of gold nanostars. For example only a broad band in the region 3000-3600 cm⁻¹ was obtained for Au nanostars whereas clear peaks corresponding to OH, CH, and NH vibrations were present for L-DOPA. In particular, the IR spectrum of the nanocrystals has quite resemblance with that reported for melanin like structures.[50,54,55] This indicates the polymeric nature of surface bound ligands. Hence, fostering of branched Au nanocrystals may occur through the shape directing action of produced polymeric structures. Such instances have been reported in similar cases.[41] Further to understand the role of L-DOPA and hence to gain insight on the nanoparticle growth mechanism, we have performed detailed absorption and microscopic studies and the results are detailed below.

Effect of L-DOPA concentration on tuning the morphology of nanocrsytals

Since L-DOPA plays the role of both reducing and stabilizing agent, modulation of its molar ratio could be a viable strategy to tune the morphology of the nanocrystals. Fig. 2 shows the colour photograph of the solution and corresponding absorption spectra of nanoparticles prepared in presence of varying amounts of L-DOPA while maintaining all other conditions constant. In about ~ 2 minutes almost all the solutions developed wine red colour, except that above 0.20 mM. As time progresses, there was drastic colour changes to each of these solutions (Fig. 2A, 2B). At very low concentrations (0.03 mM L-DOPA) solution developed red colour that got intensified over a period of 15 minutes. Only a single plasmon band with maximum around 540 nm appeared in the equivalent absorption spectrum. Similar observation was noticed when the amount of L-DOPA was raised to 0.05 mM. The solution initially attained wine red color which deepened in about 15 minutes and the absorption maximum got blue shifted to ~ 530 nm with narrowing of the band width (Fig. S5, ESI†). Along with this, the optical density (OD)
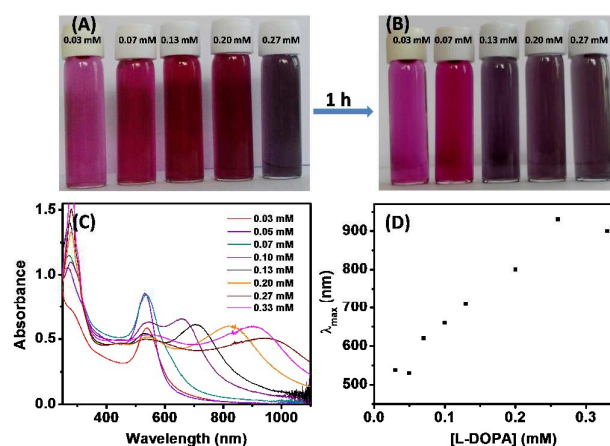

Fig. 2 (A,B) Color photographs of nanoparticle solutions prepared in presence of different L-DOPA concentrations ([L-DOPA] = 0.03-0.27) taken after (A) 2 minutes and (B) 1 h of mixing the reagents, (C) absorption spectra of nanoparticle solutions represented in photograph (B) and (D) plot showing variation of the absorption wavelength maximum with respect to L-DOPA concentration.

improved from 0.6 to 0.9 (Fig. 2C) supporting the reducing action of L-DOPA. Wherein, the raise of reductant concentration resulted in conversion of larger percentage of Au^{3+} ions to Au(0) thus producing more number of Au nanoparticles. The hypsochromic shift in absorption maximum bestow to the evolution of nanoparticles having smaller sizes. Whereas decrease in the full width at half maximum (FWHM) of the band may imply the more uniform size distribution of the nanocrystals (*vide infra*). However, with any further increase in molar ratio, over a period of time, the initially generated wine red color gradually changes to purple and grey. The optical measurements recorded after 1 hour showed a decrease in the OD at 530 nm and a new red shifted band appeared (Fig. 2C). The position of this band underwent a gradual and linear red-shift along with added reductant volume (Fig. 2D). For example, the nanomaterials prepared in the presence of 0.07 mM L-DOPA have major absorption peak at ~ 530 nm and shoulder at ~620 nm. Bathochromically shifted clear new peaks at 660, 710, 800 and 930 nm were produced when the amount of reductant reaches 0.1, 0.13, 0.2, and 0.26 mM respectively. Any further increase in molar ratio brought blue shift to the absorption maximum (λ_{max} = 900 nm for 0.33 mM). These spectral changes could be attributed to the formation of anisotropic nanostructures having different size and morphology which were further detailed through microscopic studies.

Represented in Fig. 3 and Fig. S6-S21 (ESI†) are the examples of TEM images of nanocrystals synthesized by varying the amount of L-DOPA. Nanomaterials of average size ~ 40 nm having spherical and multiply twinned structures were obtained at very low molar percentages (0.03 mM). Whereas raise in L-DOPA concentration to 0.05 mM materialized particles with more uniform sizes and reduced dimensions (~ 35 nm) (Fig. S10, ESI†). This is in consistent with our observed blue shift in the absorption maximum and shrunken FWHM value (*vide supra*) which corroborates with earlier literature reports.[56] Hence, this also substantiates the capping role of the reductant. Thus, at smaller molar ratios the amount of protecting ligand is insufficient to properly cover the nanoparticle surface thus resulting in more polydispersity. In addition, at this molar ratio, a minute percentage of (~ 5 %) tiny particles (< 10 nm) also coexists. This may additionally contributes to the obtained hypsochromic shift in the absorption maximum. Interestingly, gradual evolution of nanoparticles having other morphologies such as nanostars

and nanoflowers were evident with more added volumes of L-DOPA. For example, about 30 % of the particles formed have multiple arms when the concentration reaches ~ 0.07 mM (Fig. 3B, G). The size of the spherical nanoparticles is determined as 30-35 nm from TEM images. On the other hand contemporary nanostars are slightly bigger in dimensions (Fig. S11-S14, ESI†). Furthermore, in this case the percentage of smaller particles having dimensions < 10 nm has considerably increased when compared to that at 0.05 mM. A further increase in fraction of star shaped particles have (> 50 %) been observed when the concentration reaches 0.1 mM. However, most of the nanocrystals have < 4 number of branches and the protrusions are mainly underdeveloped (Fig. S16, ESI†). Therefore it is not surprising that this solution exhibit the lowest LSPR peak position (λ_{max} = 670 nm). More than 90 % of star shaped particles (size ~ 35 nm) were obtained when the reductant was further increased to 0.13 mM. Whereas, higher molar ratios resulted in flower like morphologies with many number of arms (petals). For example, along with star shaped materials, flowers having, mainly two layers of petals were obtained in presence of 0.2 mM L-DOPA (Fig. 3D, I). The size distribution analysis gave dimensions of ~ 40 nm for these nanostructures (Fig. S18, ESI†). A further increase in size (to ~ 50 nm) and the number of petals was perceived when the concentration reaches 0.27 mM. This is in consistent with redshift in the absorption maximum from 800 to 930 nm. HRTEM images, reveals the flower like morphologies are having arms with mainly (111) planes (Fig. S19, ESI†). Further raise in reductant concentration caused a decrease in the percentage of nanoflowers and most of the nanostructures have star shaped morphologies with size ~ 30 nm (Fig. S20, S21, ESI†). This is in accordance with the observed blue shift in LSPR band.

Kinetics studies

To gain further insight on the mechanistic aspects of multiple types of nanoparticles realization, absorption spectral changes as a function of time were recorded for each of the solutions. Upon mixing the three reagents, plasmon absorption above 530 nm was obvious in all the cases. For example, at 0.05 mM, initially a broad band was appeared at around 540 nm. With time this peak got intensified and blue shifted (to 530 nm) along with peak width sharpening. These spectral changes attained saturation stage in period of about 1 hour. This implies that initially formed nanoparticles may be having wide size distribution. As the reaction progresses more nanoparticles with uniform dimensions are evolved due to continuous reduction of Au^{3+} ions and the reorganization of the initially formed nanoparticles (*vide supra*). Similar trend has been perceived in other samples. However, at concentrations higher than 0.13 mM, more red-shifted and broad spectra were obtained for the beginning of the reaction as well as at the first saturation period. The time required for reaching the first saturation period got diminished to ~50, 20, 8 and 3 minutes respectively for 0.05, 0.1, 0.13 and 0.2 mM concentrations (Fig. 4 and Fig. S22, ESI†). As a result of this fast reduction rate, nanoparticles formed could be ill defined and are more polydisperse.[57] After the initial saturation period, the
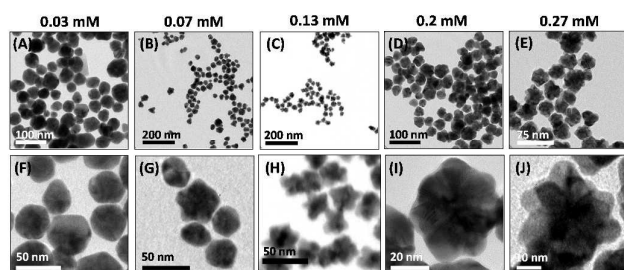

Fig. 3 Representative examples of TEM images of nanocrystals prepared by varying the amount of L-DOPA.
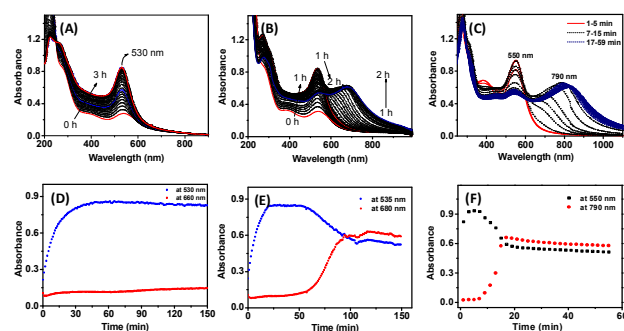
Fig. 4 (A-C) Time dependent absorption spectral changes of HAuCl₄ solution after the addition of L-DOPA; ([L-DOPA] = 0.05 mM (A), 0.1 mM (B), 0.2 mM (C). (D-E) shows the evolution of optical density at TSPR and LSPR bands of the respective solutions.

absorption profile of nanoparticles having 0.03 and 0.05 mM L-DOPA did not undergo any considerable change. In contrast, those containing L-DOPA concentrations above 0.07 mM, exhibited a continuous drop of the peak intensity at 530 nm and a new band was concomitantly emerged at lower energies.   The simultaneous occurrence of both these processes indicates transformation of initially formed nanoparticles to anisotropic nanostructures.

Mechanism

Understanding the nanoparticle formation mechanism is highly essential to materialize control over their size and morphology and tailoring their properties to desired applications.[45,57-59] However, the limitations posed by (i) the absence of a well-defined externally added seed, (ii) relatively faster reaction rate, (iii) the inability to trap the intermediate stages of growth and (iv) and the possible solid state reactions/coalescence occurred during solvent evaporation and drying on TEM grid has restricted us in arriving at any concrete assumption on the mechanism. From the microscopic studies it was evident that spheroid nanostructures are produced at lower molar ratios and multi-branched particles at higher ones. This may signifies soft templating role of the capping ligand. In fact, the nature of surface bound ligands is estimated from IR studies as polymeric product of L-DOPA oxidation (*vide supra*). This is also fortified by the detection of an organic shell around nanoparticles in majority of the TEM images (Fig. S23, ESI†). Formation of anisotropic nanostructures has been reported in presence of such bio-polymeric materials.[41] In most of the well established procedures, the synthesis of anisotropic nanostructures were achieved by the over growth of small nanoparticles (commonly termed as nanoseeds) with the aid of soft templates like CTAB and AgNO₃.[8,60,61] In such instances, shape directing agents adsorbs on certain planes of the nanoseeds thus blocking further growth along these sides. Then the formation of anisotropic nanostructure occurs via expansion of the exposed facets. This is accompanied by a continuous and simultaneous progression of absorption in the entire plasmon region. Because, the anisotropic nanostructures have much higher extinction coefficient compared to the spherical nanoparticles of the same size.[10,62] On the other hand, the approach described here, is devoid of

the use of nanoseeds or any conventional shape directing agents. Even if nanoseeds are produced in the initial stages of the reaction, and the anisotropic nanostructures are generated via their simple over growth, one would expect similar trend in the absorption spectra. However in the present case, it is noticed (i) first the evolution of a band around 530 nm, indicating that the initially formed nanoparticles are spherical in shape (ii) which then gradually decreases in intensity along with the concomitant formation of a low energy absorption. Earlier theoretical and experimental studies have given evidence to the red-shifting of absorption maximum when two nanoparticles come close to each other. The peak position of this new band is highly dependent on the number of particles and the distance between them.[63-65] The sigmoidal nature of the LSPR absorption evolution indicates the multi-branched nanostructure realization described here is autocatalytic in nature.[66] This, involves at least three stages (Fig. 5) (i) Booming of smaller nanoparticles having size < 10 nm (ii) their agglomeration and (iii) followed by their overgrowth to well defined nanostructures. This proposition is reinforced by several facts and are detailed as follows. (i) Large percentage of smaller particles has been found both in the DLS and TEM images at the first saturation period. (ii) Several distinct agglomerates of small particles were observed in different areas of TEM gird. The analysis of the kinetic data disclosed minimum 2.5 times higher rate for increase in LSPR absorption than the drop of optical density at 530 nm. This is because, formation of one nanostar requires agglomeration of many number of particles. Hence the absorption spectral changes due to decrease in the number of individualized small particles overwhelms the effect caused by high extinction coefficient of branched nanocrystals. (iii) A systematic examination of both TEM images and DLS data illustrated a raise in overall size in the LSPR growth stage along with time (Fig. S24, ESI†). Thus according to this mechanism it could be assumed that the morphology of final nanostructure is dictated by the initial aggregation number. The kinetic studies expressed an increase in reaction rate with raise in L-DOPA concentration. This implies the number of particles present at a particular time in a given volume will be proportional to the reductant concentration. This in turn affects the initial aggregation number which varies in the order 0.03 = 0.5 > 0.1 > 0.13 > 0.16 > 0.2 > 0.27 mM.   After this initial aggregation process, growth process occurs mainly at the exposed facets and the HRTEM images revealed, the arms of the multibranched nanocrystals
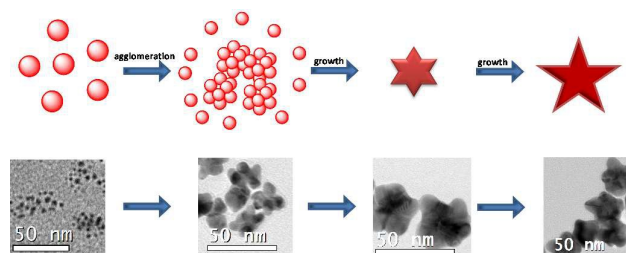

Fig. 5 Schematic representation (up) and illustrative examples of TEM images showing the evolution of branched nanocrystals via particle agglomeration and growth process.

are mainly (111) facets. It could also be pointed out that effect of L-DOPA concentration on the size of nanocrystals may appear self-contradictory. There was a reduction in the average particle size from 40 nm to 35 nm when the L-DOPA concentration was raised from 0.03 to 0.05 mM. There after particle size got steadily increased to 40 and 50 nm for 0.2 and 0.27 mM reductant concentrations respectively (*vide supra*). However it is to be noted that the particle morphology is entirely different for these concentration regimes. Only spheroid particles are observed at lower concentrations whereas the nanocrystals formed have multiple arms that above 0.1 mM. Moreover the kinetic studies presented here (Figure 4 and Fig. S22, ESI†) demonstrate a clear difference in their formation mechanism. Only continuous evolution plasmon absorption at ~ 530 nm was observed for spheroid particles. i.e. they are formed by the overgrowth of initially formed nuclei. On the contrary, at concentration above 0.1 mM, the kinetic plot shows three distinct stages (i) fast raise in absorbance at ~ 530 nm (ii) then an induction period (iii) followed by evolution of low energy LSPR band by the deprivation of the initially formed peak at 530 nm. Thus the multi-branched nanocrystals are materialized through an aggregative growth mechanism at the expense of the initially formed spherical particles which serve as seeds.[58,59] Hence it could be argued that the final size and morphology of these nanocrystals is dictated by the aggregation number rather than only capping ligand concentration (*vide supra*). The average number of arms of the produced nanocrystals varies as 0, 5, 12 and 18 for concentrations 0.03 (and 0.05), 0.13, 0.2 and 0.26 mM concentrations respectively and could be grown from an equivalent no. of agglomerating particles. At larger added volumes the diminishing of the particle size could be due to the combined effects of decrease in effective nanoparticle concentration (arising from volume change) and increase in the capping ligand concentrations. In the nanoparticles synthesis it is generally known that large percentage of the capping ligand reduces the particle size.

Conclusions

In conclusion, the potentiality of L-DOPA for a versatile seedless and surfactantless one pot room temperature synthetic strategy for the preparation of multiple types of Au nanocrystals has been developed. Tuning the shape and the optical properties of the nanocrystals was accomplished by simple variation of the reductant concentration. This together with, FTIR studies and the observation of organic shell around the nanomaterials confirm the bifunctional role of L-DOPA. Analysis of the kinetic data and the microscopic images revealed that formation of different types of nanocrystals proceeds through spherical nanoparticles which then aggregates and overgrows into nanoparticles of specific shape. L-DOPA is an important biomolecule and is a precursor to several neurotransmitters including dopamine. Since the present methodology is devoid of any toxic surfactants and being a biocompatible molecule is used for preparation, the nanomaterials thus produced could be highly suitable for

biomedical applications. Together with this, their tunable NIR absorption, relatively smaller sizes (30-60 nm), presence of multiple branches indicate their potential for sensing and therapeutic applications. One of the main design strategy adopted in the present work is the bifunctional role played by L-DOPA. i.e. structurally it contains a stabilizing and reducing parts and there are several other biomolecules in nature incorporating these functions (eg. Caffaeic acid). Therefore we believe that the methodology presented here opens up newer possibilities of making biocompatible anisotropic nanomaterials with similar biomolecules which may find application in both sensing and bio-medicinal fields.

Acknowledgements

References

1. J. Lee, B. Hua, S. Park, M. Ha, Y. Lee, Z. Fan and H. Ko, *Nanoscale*, 2014, **6**, 616-623.
2. K. Jung, J. Hahn, S. In, Y. Bae, H. Lee, P. V. Pikhitsa, K. Ahn, K. Ha, J.-K. Lee, N. Park and M. Choi, *Adv. Mater.*, 2014, **26**, 5924-5929.
3. V. W. K. Ng, R. Berti, F. Lesage and A. Kakkar, *J. Mater. Chem. B*, 2013, **1**, 9-25.
4. M. A. Mackey, M. R. K. Ali, L. A. Austin, R. D. Near and M. A. El-Sayed, *J. Phys. Chem. B*, 2014, **118**, 1319-1326.
5. J. Kumar, R. Thomas, R. S. Swathi and K. G. Thomas, *Nanoscale*, 2014, **6**, 10454-10459.
6. S. Lal, N. K. Grady, J. Kundu, C. S. Levin, J. B. Lassiter and N. J. Halas, *Chem. Soc. Rev.*, 2008, **37**, 898-911.
7. H. Yuan, C. G. Khoury, H. Hwang, C. M. Wilson, G. A. Grant and T. Vo-Dinh, *Nanotechnology*, 2012, **23**, 075102.
8. Q. Zhang, N. Large and H. Wang, *ACS Appl. Mater. Interfaces*, 2014, **6**, 17255-17267.
9. X.-L. Liu, J.-H. Wang, S. Liang, D.-J. Yang, F. Nan, S.-J. Ding, L. Zhou, Z.-H. Hao and Q.-Q. Wang, *J. Phys. Chem. C*, 2014, **118**, 9659-9664.
10. H. de Puig, J. O. Tam, C.-W. Yen, L. Gehrke and K. Hamad-Schifferli, *J. Phys. Chem. C*, 2015, **119**, 17408–17415.
11. L. Rodríguez-Lorenzo, R. A. Álvarez-Puebla, I. Pastoriza-Santos, S. Mazzucco, O. Stéphan, M. Kociak, L. M. Liz-Marzán and F. J. García de Abajo, *J. Am. Chem. Soc.*, 2009, **131**, 4616-4618.
12. M. Chirumamilla, A. Toma, A. Gopalakrishnan, G. Das, R. P. Zaccaria, R. Krahne, E. Rondanina, M. Leoncini, C. Liberale, F. De Angelis and E. Di Fabrizio, *Adv. Mater.*, 2014, **26**, 2353-2358.
13. S. Harmsen, M. A. Bedics, M. A. Wall, R. Huang, M. R. Detty and M. F. Kircher, *Nat. Commun.*, 2015, **6**, 6570.

14. L. Dykman and N. Khlebtsov, *Chem. Soc. Rev.*, 2012, **41**, 2256-2282.

15. T. K. Sau and C. J. Murphy, *J. Am. Chem. Soc.*, 2004, **126**, 8648-8649.

16. H.-Y. Wu, M. Liu and M. H. Huang, *J. Phys. Chem. B*, 2006, **110**, 19291-19294.

17. M. Yamamoto, Y. Kashiwagi, T. Sakata, H. Mori and M. Nakamoto, *Chem. Mater.*, 2005, **17**, 5391-5393.

18. C. G. Khoury and T. Vo-Dinh, *J. Phys. Chem. C*, 2008, **112**, 18849-18859.

19. P. S. Kumar, I. Pastoriza-Santos, B. Rodríguez-González, F. J. G. d. Abajo and L. M. Liz-Marzán, *Nanotechnology*, 2008, **19**, 015606.

20. C.-H. Kuo and M. H. Huang, *Langmuir*, 2005, **21**, 2012-2016.

21. P. Pallavicini, A. Dona, A. Casu, G. Chirico, M. Collini, G. Dacarro, A. Falqui, C. Milanese, L. Sironi and A. Taglietti, *Chem. Commun.*, 2013, **49**, 6265-6267.

22. S. Umadevi, H. C. Lee, V. Ganesh, X. Feng and T. Hegmann, *Liq. Cryst.*, 2014, **41**, 265-276.

23. J. Xie, J. Y. Lee and D. I. C. Wang, *Chem. Mater.*, 2007, **19**, 2823-2830.

24. G. Maiorano, L. Rizzello, M. A. Malvindi, S. S. Shankar, L. Martiradonna, A. Falqui, R. Cingolani and P. P. Pompa, *Nanoscale*, 2011, **3**, 2227-2232.

25. H. Liu, Y. Xu, Y. Qin, W. Sanderson, D. Crowley, C. H. Turner and Y. Bao, *J. Phys. Chem. C*, 2013, **117**, 17143-17150.

26. E. Hao, R. C. Bailey, G. C. Schatz, J. T. Hupp and S. Li, *Nano Lett.*, 2004, **4**, 327-330.

27. Q. Liu, L. Lai, H. Huang, J. Sun, T. Shang, Q. Zhou and Z. Xu, *Chin. J. Chem.*, 2010, **28**, 537-542.

28. A. Kedia and P. Senthil Kumar, *J. Phys. Chem. C*, 2011, **116**, 1679-1686.

29. R. He, Y.-C. Wang, X. Wang, Z. Wang, G. Liu, W. Zhou, L. Wen, Q. Li, X. Wang, X. Chen, J. Zeng and J. G. Hou, *Nat. Commun.*, 2014, **5**, 4327.

30. L.-C. Cheng, J.-H. Huang, H. M. Chen, T.-C. Lai, K.-Y. Yang, R.-S. Liu, M. Hsiao, C.-H. Chen, L.-J. Her and D. P. Tsai, *J. Mater. Chem.*, 2012, **22**, 2244-2253.

31. R. Baron, M. Zayats and I. Willner, *Anal. Chem.*, 2005, **77**, 1566-1571.

32. K. Yoosaf, B. I. Ipe, C. H. Suresh and K. G. Thomas, *J. Phys. Chem. C*, 2007, **111**, 12839-12847.

33. M. Reza Hormozi Nezhad, J. Tashkhourian, J. Khodaveisi and M. Reza Khoshi, *Anal. Methods*, 2010, **2**, 1263-1269.

34. J. A. Ho, H.-C. Chang and W.-T. Su, *Anal. Chem.*, 2012, **84**, 3246-3253.

35. C. Jiang, M. Ma and Y. Wang, *Anal. Methods*, 2012, **4**, 3570-3574.

36. I. Baginskiy, T.-C. Lai, L.-C. Cheng, Y.-C. Chan, K.-Y. Yang, R.-S. Liu, M. Hsiao, C.-H. Chen, S.-F. Hu, L.-J. Her and D. P. Tsai, *J. Phys. Chem. C*, 2013, **117**, 2396-2410.

37. W.-G. Qu, S.-M. Wang, Z.-J. Hu, T.-Y. Cheang, Z.-H. Xing, X.-J. Zhang and A.-W. Xu, *J. Phys. Chem. C*, 2010, **114**, 13010-13016.

38. L. Zhang, K. Xia, Z. Lu, G. Li, J. Chen, Y. Deng, S. Li, F. Zhou and N. He, *Chem. Mater.*, 2014, **26**, 1794-1798.

39. G. Su, C. Yang and J.-J. Zhu, *Langmuir*, 2015, **31**, 817-823.

40. J. Li, J. Wu, X. Zhang, Y. Liu, D. Zhou, H. Sun, H. Zhang and B. Yang, *J. Phys. Chem. C*, 2011, **115**, 3630-3637.

41. S. Yi, L. Sun, S. C. Lenaghan, Y. Wang, X. Chong, Z. Zhang and M. Zhang, *RSC Advances*, 2013, **3**, 10139-10144.

42. H. Lee, S. M. Dellatore, W. M. Miller and P. B. Messersmith, *Science*, 2007, **318**, 426-430.

43. A. Kedia and P. S. Kumar, *RSC Adv.*, 2014, **4**, 4782-4790.

44. L. Rodríguez-Lorenzo, R. de la Rica, R. A. Álvarez-Puebla, L. M. Liz-Marzán and M. M. Stevens, *Nat. Mater.*, 2012, **11**, 604-607.

45. Y. Xia, Y. Xiong, B. Lim and S. E. Skrabalak, *Angew. Chem. Int. Ed.*, 2009, **48**, 60-103.

46. A. Manjavacas and F. J. García de Abajo, *Nat. Commun.*, 2014, **5**, 3548.

47. H. Wang, D. W. Brandl, P. Nordlander and N. J. Halas, *Acc. Chem. Res.*, 2007, **40**, 53-62.

48. F. Hao, C. L. Nehl, J. H. Hafner and P. Nordlander, *Nano Lett.*, 2007, **7**, 729-732.

49. S. Moulay, *Polym. Rev.*, 2014, **54**, 436-513.

50. M. Apte, G. Girme, A. Bankar, A. RaviKumar and S. Zinjarde, *J Nanobiotechnology*, 2013, **11**, 2.

51. Y. Zhou, R. Alany, V. Chuang and J. Wen, *Chromatographia*, 2012, **75**, 597-606.

52. J. Rodríguez-Fernández, J. Pérez-Juste, P. Mulvaney and L. M. Liz-Marzán, *J. Phys. Chem. B*, 2005, **109**, 14257-14261.

53. M. Eslami, H. R. Zare and M. Namazian, *J. Phys. Chem. B*, 2012, **116**, 12552-12557.

54. A. Banerjee, S. Supakar and R. Banerjee, *PLoS ONE*, 2014, **9**, e84574.

55. M. T. Shaaban, S. M. M. El-Sabbagh and A. Alam, *Life Sci. J.*, 2013, **10**, 1437-1448.

56. G. Frens, *Nature, Phys. Sci.*, 1973, **241**, 20–22.

57. Y. Xia, X. Xia and H.-C. Peng, *J. Am. Chem. Soc.*, 2015, **137**, 7947-7966.

58. F. Wang, V. N. Richards, S. P. Shields and W. E. Buhro, *Chem. Mater.*, 2014, **26**, 5-21.

59. N. T. K. Thanh, N. Maclean and S. Mahiddine, *Chem. Rev.*, 2014, **114**, 7610-7630.

60. M. R. Langille, M. L. Personick, J. Zhang and C. A. Mirkin, *J. Am. Chem. Soc.*, 2012, **134**, 14542-14554.

61. M. Grzelczak, J. Perez-Juste, P. Mulvaney and L. M. Liz-Marzan, *Chem. Soc. Rev.*, 2008, **37**, 1783-1791.

62. R. D. Near, S. C. Hayden, R. E. Hunter, D. Thackston and M. A. El-Sayed, *J. Phys. Chem. C*, 2013, **117**, 23950-23955.

63. Z. Zhong, S. Patskovskyy, P. Bouvrette, J. H. T. Luong and A. Gedanken, *J. Phys. Chem. B*, 2004, **108**, 4046-4052.

64. J. Kumar and K. G. Thomas, *J. Phys. Chem. Lett.*, 2011, **2**, 610-615.

65. L. O. Herrmann, V. K. Valev, C. Tserkezis, J. S. Barnard, S. Kasera, O. A. Scherman, J. Aizpurua and J. J. Baumberg, *Nat. Commun.*, 2014, **5**, 4568.

66. C. Besson, E. E. Finney and R. G. Finke, *J. Am. Chem. Soc.*, 2005, **127**, 8179-8184.

Microscopic and spectroscopic analysis of multiple types of nanocrystal formation in a one pot seedless and surfactantless procedure